

Hydrogeological flow patterns and hydrochemical driving forces of groundwater in a typical coastal hilly region of the Jinjiang watershed, Southeast China: Recommendations for water pollution control and management

Zhong-shuang Cheng, Chen Su, Wen-zhong Wang, Bing-yan Li, En-de Zuo, Yu-meng Tian, Zhao-xian Zheng

Citation: Zhong-shuang Cheng, Chen Su, Wen-zhong Wang, Bing-yan Li, En-de Zuo, Yu-meng Tian, Zhao-xian Zheng, 2026. Hydrogeological flow patterns and hydrochemical driving forces of groundwater in a typical coastal hilly region of the Jinjiang watershed, Southeast China: Recommendations for water pollution control and management, China Geology, 9, 316-332. doi: 10.31035/cg2024185.

View online: https://doi.org/10.31035/cg2024185

Related articles that may interest you

Characteristics and sources of microplastic pollution in the water and sediments of the Jinjiang River Basin, Fujian Province, China
China Geology. 2022, 5(3), 429 https://doi.org/10.31035/cg2022051

Changes of groundwater flow field of Luanhe River Delta under the human activities and its impact on the ecological environment in the past 30 years
China Geology. 2021, 4(3), 455 https://doi.org/10.31035/cg2021060

Determining the groundwater basin and surface watershed boundary of Dalinuoer Lake in the middle of Inner Mongolian Plateau, China and its impacts on the ecological environment
China Geology. 2021, 4(3), 498 https://doi.org/10.31035/cg2021066

Analysis of debris flow control effect and hazard assessment in Xinqiao Gully, Wenchuan M_s 8.0 earthquake area based on numerical simulation
China Geology. 2024, 7(2), 248 https://doi.org/10.31035/cg2023144

Groundwater metal pollution and health risk assessment in river valley heavy industrial cities of arid regions in China
China Geology. 2025, 8(3), 526 https://doi.org/10.31035/cg2025084

Distribution, characteristics and influencing factors of fresh groundwater resources in the Loess Plateau, China
China Geology. 2021, 4(3), 509 https://doi.org/10.31035/cg2021057

China Geology 9 (2026) 316−332

China Geology

Journal homepage: http://chinageology.cgs.cn
https://www.sciencedirect.com/journal/china-geology



Hydrogeological flow patterns and hydrochemical driving forces of groundwater in a typical coastal hilly region of the Jinjiang watershed, Southeast China: Recommendations for water pollution control and management

Zhong-shuang Cheng[a, b, c], Chen Su[a, b], Wen-zhong Wang[a, b,*], Bing-yan Li[a, b], En-de Zuo[a, b], Yu-meng Tian[d], Zhao-xian Zheng[a, b,*]

[a] *Institute of Hydrogeology and Environmental Geology, Chinese Academy of Geological Sciences, China Geological Survey, Ministry of Natural Resources, Xiamen* 361021, *China*
[b] *Key Laboratory of Groundwater Science and Engineering, Ministry of Natural Resource, Shijiazhuang* 050061, *China*
[c] *Fujian Provincial Key Laboratory of Water Cycling and Eco-Geological Processes, Xiamen* 361021, *China*
[d] *College of Earth Sciences, Jilin University, Changchun* 130061, *China*

ARTICLE INFO

Article history:
Received 25 November 2024
Received in revised form 7 March 2025
Accepted 30 March 2025
Available online 3 September 2025

Keywords:
Groundwater flow pattern
Atmospheric precipitation
Hydrochemistry
Nitrate
Driving forces
Seawater intrusion
Electrochemical sensor networks
Machine learning
Coastal area
Sustainable Development Goal (SDG)
Groundwater management
Hydrogeological survey engineering

ABSTRACT

Coastal groundwater (CGW) systems in rapidly urbanizing regions face critical challenges in achieving Sustainable Development Goal (SDG), where anthropogenic pressures intersect with hydrogeological vulnerability. This study employs coupled isotopic-hydrogeochemical analysis and geostatistics to unravel hydrochemical driving forces compromising groundwater quality in the Jinjiang Downstream Watershed (DJW), Southeast China. The results indicated that groundwater was predominantly recharged from local atmospheric precipitation and lateral recharge from the adjacent boundaries. Hydrochemical distributions exhibited a distinct pattern, transitioning from HCO_3-Ca to HCO_3·Cl-Ca, and then to Cl-Mg·Ca/Na·Ca, reflecting processes ranging from freshwater recharge to seawater intrusion (SWI). Elevated nitrates were primarily attributed to domestic sewage leakage and septic tank leaching. Additionally, preferential flow posed a risk to deep groundwater quality, by facilitating the rapid transport of contaminants through rock fractures. Key driving forces of hydrochemistry included silicate dissolution with local runoff paths, SWI, and human activities. The study advocates for a governance paradigm integrating electrochemical sensor networks with machine learning-driven contaminant prediction and phased membrane bioreactor deployment, which synergistically reduce nitrate fluxes while maintaining aquifer freshening processes. This integrated approach establishes a scalable model for SDG-aligned groundwater management in vulnerable coastal zones, demonstrating how process-based insights can bridge scientific discovery and water security implementation.

©2026 China Geology Editorial Office.

1. Introduction

Freshwater scarcity poses a critical constraint on socioeconomic development in coastal areas, where water demand often exceeds supply due to rapid population growth, urbanization, and intensive agricultural practices (Luijendijk E et al., 2020; Han DM and Currell MJ, 2022; Zamrsky Z et al., 2024). Coastal groundwater (CGW), a vital freshwater resource sustaining over 40% of global coastal populations (UNESCO, 2022), plays dual roles in supporting human society and maintaining fragile coastal ecohydrological system (Luijendijk E et al., 2020; Liu CL et al., 2021; Huang GX and Li LP, 2024). Yet, Sustainable Development Goal 6 (SDG 6, Clean Water and Sanitation) remains unattainable in many coastal zones as CGW faces compounding threats: Contamination from urbanization/agriculture (Liu JT et al., 2024), seawater intrusion (SWI, Gao ZJ et al., 2021), and climate-driven hydrological shifts (Richardson CM et al., 2024; Schroeter SA et al., 2025). These pressures degrade water usability for drinking, agriculture, and industry, while jeopardizing SDG 3 (Good Health) through chronic exposure to nitrate and heavy metals (Lin L and Pussella P, 2017; Fu TF et al., 2022). Understanding the hydrochemical drivers and

First author: *E-mail address*: zshuangcheng@163.com (Zhong-shuang Cheng).

* Corresponding author: *E-mail address*: wwenzhong2005@163.com (Wen-zhong Wang); aslangyeah@126.com (Zhao-xian Zheng).

Literary editor: Li-qiong Jia
doi:10.31035/cg2024185
2096-5192/© 2026 China Geology Editorial Office.

flow dynamics of CGW is thus imperative for bridging the gap between water security goals and on-ground realities.

The hydrochemical evolution of CGW reflects both natural geological processes and escalating anthropogenic impacts (Han DM et al., 2016; Morici S et al., 2023; Liu JT et al., 2024). Coastal regions are typically discharge zones for onshore groundwater systems, accumulating salts and pollutants and integrating upstream water quality impacts. This has led to more severe groundwater quality deterioration in coastal areas compared to inland groundwater flow systems (Rodell M et al., 2018; Amiri V et al., 2023; Zhang F et al., 2023). Furthermore, the intensity of human activities in these regions, further degraded the water quality, such as nitrate-N concentrations exceeding WHO limits by 3–8 times (Lingle DA et al., 2017; Luo MH et al., 2023; Moussaoui I et al., 2023). Such contamination patterns mirror global trends where coastal aquifers act as terminal sinks, accumulating pollutants from upstream catchments (Amiri V et al., 2023; Zhang Y et al., 2023). In addition, short groundwater flow paths in hilly terrains enable rapid pollutant transfer from land surface to coastal discharge zones (Huang GX and Li LP, 2024). This underscores the need for spatially explicit management frameworks that account for coastal hydrogeological uniqueness.

Last researches have emphasized integrating multi-tracer techniques (isotopes, hydro geochemistry) to disentangle natural and anthropogenic influences (Wang H et al., 2021; Richardson CM et al., 2024; Zamrsky Z et al., 2024). However, critical knowledge gaps persist in humid coastal regions like southeastern China, where evolution and driving forces of hydrochemistry remain understudied. It limited the deployment of enable real-time detection for contamination.

The downstream area of the Jinjiang watershed (DJW), exemplifies these challenges, characterized by low-lying terrain surrounded by mountains and facing the sea, as it undergoes rapid urbanization and industrialization (Fig. 1). In this area, groundwater serves as an important secondary and emergency water source, with a close relationship to surface water systems (Lu YX and Zhang JM, 2010; Zhu JC et al., 2018). Thin aquifers, short groundwater runoff paths and rapid circulation in the DJW significantly differ from those in the large plain of North China (Li CC et al., 2020; Cheng ZS et al., 2021; Kwon HI et al., 2022). Additionally, elevated levels of NO_3^- have been reported in both groundwater and surface water in the DJW (Han DM and Currell MJ, 2022; Li ZH et al., 2024; Zhu YC et al., 2024). Despite documented nitrate pollution, systematic analyses of hydrochemical driving mechanisms (including nitrate contamination), and SWI remain lacking.

This study addresses these gaps through comprehensively investigating a coupled hydrogeochemical and isotopic investigation of DJW's coastal aquifer system. By elucidating hydrochemical evolution and driving forces to optimize monitoring for hazardous pollutants, the authors provide actionable insights for achieving SDG targets in similar coastal settings.

2. Materials and methods

2.1. Geology and hydrogeology

The research area is situated downstream of the Jinjiang River, around Quanzhou City in Southeast China, along the coast of the East China Sea (Fig. 1a). The region is characterized by low mountains and hilly terrain, with topography primarily influenced by regional geological structures and diverse lithological formations. Climatically, the area features a subtropical marine monsoon climate characterized by warm, and humid conditions and abundant perennial rainfall. Annual temperature ranges from 18°C to 22°C, and annual precipitation varies between 1000 mm and 1800 mm. The Jinjiang River, a perennial stream originating from Daiyun Mountain outside the northwest of research area, flows southeastward into the East China Sea. Notably, a major tributary of the Jinjiang River is Ninety-nine Xi (99 xi) within the study area (Fig. 1a).

The Quaternary geological development is structurally controlled by NW-trending and NE-trending faults. These fractures are potential dominant channels for groundwater. Surface geology is dominated by Jurassic tuff, andesitic rocks, Quaternary sediments, volcanic sequences, and intrusive rocks (Zhu JC et al., 2018). Groundwater is reserved in interconnected pore spaces and fractures, forming three distinct aquifer types: (1) Alluvial aquifers (Aquifer 1), (2) slope pore-fissure aquifers (Aquifer 2), and (3) fissured aquifers (Aquifer 3).

Alluvial aquifers (Aquifer 1): Primarily comprising flood sand, gravel, pebble (drift) stone, aeolian sand, and marine sand, with thicknesses ranging from less than 1 m to 22 m. These aquifers are unconfined, except for a confined aquifer in Quanzhou Bay (Fig. 1b). Specific yield (Sy) values vary spatially with 15–650 m^3/d in the plain areas and 10–25 L/s in the distal fan mountains.

Slope pore-fissure aquifers (Aquifer 2): Developed within highly weathered tuff and andesitic rocks and volcanic and intrusive rocks, they are unconfined with thicknesses of less than 30 m. Specific yield (Sy) ranges from 50 m^3/d to 180 m^3/d, with spring discharges of 0.05–0.45 L/s. These aquifers provide freshwater primarily for domestic and emergency use.

Fissured aquifers (Aquifer 3): Localized in the fracture zone with well-developed bedrock joints, structural cracks, and tensile cracks, these aquifers exhibit heterogeneous hydraulic properties. Water-rich zones are concentrated near fault systems, reflecting structural controls on permeability.

Three groundwater flow systems (FS1–FS3) were delineated based on topographic, geological, and hydrodynamic constraints: (1) System boundaries are defined by surface watersheds with positive topography under favorable structural conditions. (2) Development is governed by the interplay of terrain, lithology, and hydrodynamic gradients. FS1 is situated in the northern region of the research area, along the Jinjiang River, and in close proximity to Quanzhou Bay; groundwater flow system II (FS2) is located in the southeastern region of the research area near

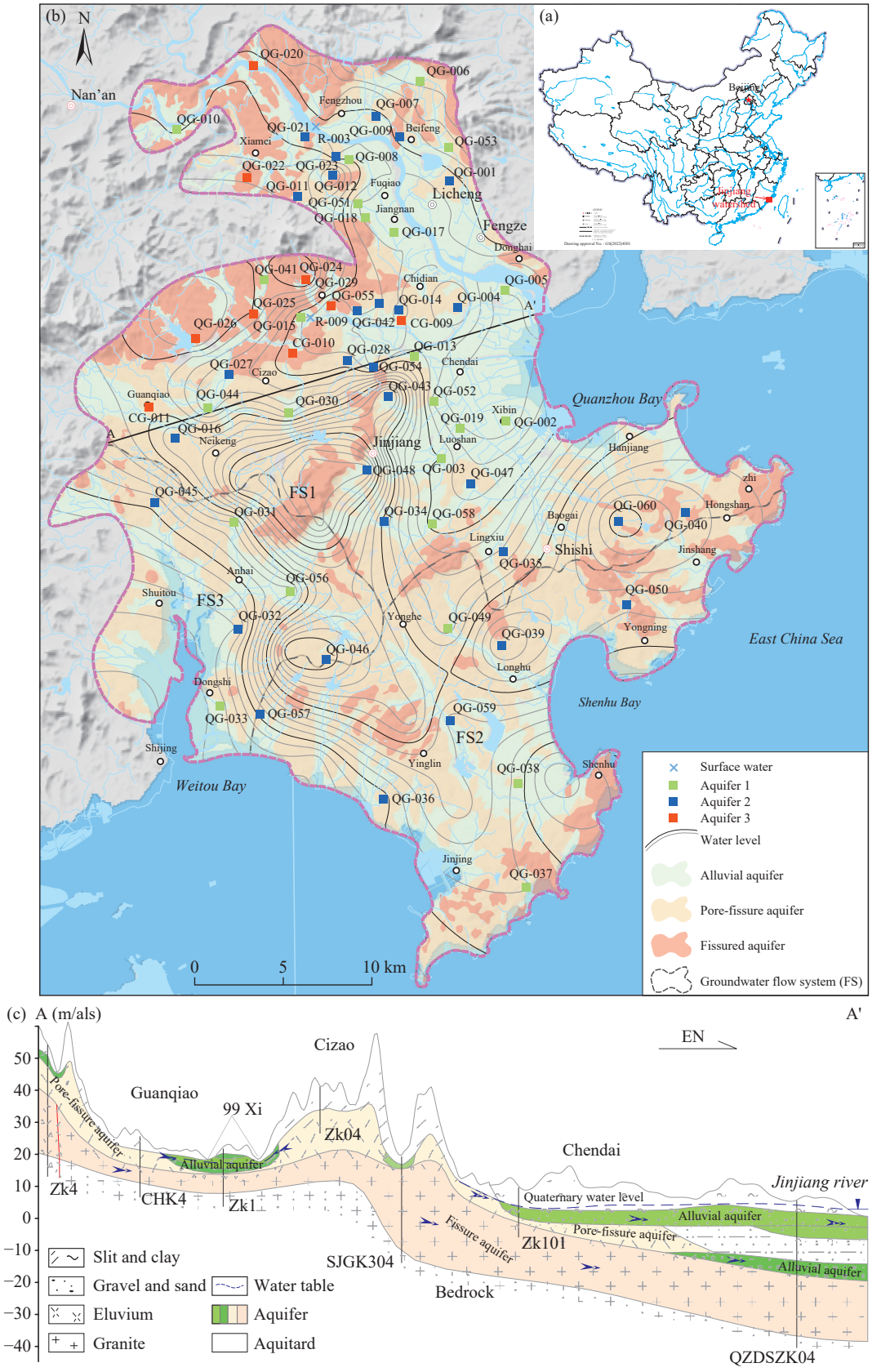


Fig. 1. a–Study area located in China; b–sampling sites with hydrological setting, groundwater flow systems; c–hydrogeologic cross-section A–A'.

Shenhu Bay; meanwhile, groundwater flow system III (FS3) is situated in the southwestern offshore area close to Weitou Bay (Fig. 1a). The overall terrain of the research area shows relatively higher elevations in the west and central parts, and relatively lower elevations along the coastal edge (Fig. 1a).

Groundwater flow directions, inferred from water table,

generally follow regional topographic gradients, transitioning from inland to coastal zones and migrating from fissured aquifers through slope pore-fissure systems to alluvial deposits (Fig. 1a). But the direction of groundwater flow significantly varies throughout the different flow systems. In FS1, flow converges westward/north-westward toward Quanzhou Bay, while FS2 exhibits southeast-to-northwest flow. Near flow system boundaries, abrupt directional shifts occur, notably in the southern research region where groundwater follows short-path northeast-to-southwest trajectories.

Obviously, the three hydrogeological units are distinguished primarily by their spatial location and the direction of groundwater flow. They are otherwise similar in terms of recharge and discharge conditions, as well as aquifer characteristics.

2.2. Sampling and analytical techniques

A total of 58 groundwater samples were collected (48 from FS1, 6 from FS2 and 4 from FS3), including 21 samples from alluvial aquifers (Aquifer 1), 28 samples from residual slope pore-fissure aquifers (Aquifer 2), and 9 samples from fissured aquifers (Aquifer 3). Additionally, 2 surface water samples were obtained (Fig. 1). The samples were extracted via a submersible pump, followed by onsite filtration with a 0.45 μm membrane. The samples were then stored and transported at a low temperature of 4°C until laboratory procedures were conducted. The analysis of the water samples included twelve chemical parameters [pH, total dissolved solids (TDS), K^+, Na^+, Ca^{2+}, Mg^{2+}, Cl^-, SO_4^{2-}, HCO_3^-, NO_3^-, NH_4^+, and F^-] and three isotopes (^3H, ^2H, and ^{18}O).

The pH was measured onsite via a multiparameter water quality tester (DZB-712F). All other analyses were conducted at the Institute of Hydrogeology and Environmental Geology, Chinese Academy of Geological Sciences (IHEG, CAGS). HCO_3^- was obtained through acid–base titration. NH_4^+, Cl^-, NO_3^-, SO_4^{2-} and F^- were quantified via the molybdenum blue spectrophotometric method. Major cations (such as K^+, Na^+, Ca^{2+}, and Mg^{2+}) were determined via inductively coupled plasma–atomic emission spectrometry (ICP-AES) via a Thermo Scientific ICAP 6300 ICP spectrometer. TDS was measured via the method of gravimetry. The accuracy of ion measurements was assessed by utilizing the absolute error in ionic equilibrium, and the error was ensured to be within 3%. The stable isotope ratios of oxygen and hydrogen were measured with a Finnigan MAT 253. The isotopic compositions were reported in δ notation expressed as per mil (‰) from the Vienna standard mean ocean water (V-SMOW). The precision for δ^2H and $\delta^{18}O$ values was ±1.0‰ and ±0.2‰, respectively. Tritium values were measured via the liquid scintillation counting method (6220 Quantulus) after electrolytic enrichment, with results presented in tritium units (TUs) and a typical error of ±0.1 TU.

2.3. Principal component analysis

In this study, principal component analysis (PCA) and hierarchical cluster analysis (HCA) were systematically applied to the groundwater hydrochemical datasets to elucidate the hydrogeochemical processes, SWI, and potential sources of nitrate (Reyment RA and Davis JC, 1988; Huang GX et al., 2018; Liu RN et al., 2024). All statistical calculations were performed in Python 3 (Python Software Foundation) using scikit-learn and SciPy libraries.

PCA served as a dimensionality reduction tool to identify the dominant factors controlling hydrochemical variations (Hou QX et al., 2020; Su H et al., 2023). The primary factor was rotated via the maximum variance, and only the principal factors were retained for analysis when eigenvalues exceeded 1. Data suitability was rigorously validated through Kaiser-Meyer-Olkin (KMO) test (>0.5) and Bartlett's sphericity test (p<0.05), ensuring robust factor extraction (Anaman R et al., 2022; Zhou J et al., 2022).

Complementarily, the hydrochemical parameters were also clustered and analysed via HCA. The average linkage method between groups was chosen, and interval measurements were conducted using the Pearson correlation coefficient. Moreover, the data underwent normalization through min-max scaling (0–1 range) conversion process (Egbueri JC, 2020).

3. Results

3.1. Hydrochemistry and isotope characteristics

Comprehending the chemical properties of groundwater is imperative for qualitatively identifying potential hydrochemical processes and hydraulic connections among aquifers. TDS serves as a key parameter that comprehensively reflects water quality in various aquifer types. For the alluvial aquifers, TDS levels ranged from 230.0 mg/L to 5980.0 mg/L, averaging at 842.6 mg/L. The residual slope pore-fissure aquifers presented TDS levels ranging from 97.0 mg/L to 870.0 mg/L, with an average of 365.6 mg/L. Similarly, the fissured aquifers presented TDS levels ranging from 87.0 mg/L to 1849.0 mg/L, averaging at 465.0 mg/L. The majority of samples were classified as freshwater (TDS < 1000 mg/L), while salinization was indicated in only a few samples primarily those in close proximity to the ocean. The predominantly natural groundwater flow regime was the primary reason for the limited salinization, which is supported by the dominant flow direction from hills to the sea (Fig. 1a). The pH values of all the groundwater samples fell within the range of 4.65 to 7.78, averaging at 6.57, indicating a generally neutral character. Meanwhile, the mean hydrochemical concentrations revealed decrease from Aquifer 1 to Aquifer 3 (Fig. 2).

The average concentrations of dominant cations in the groundwater were ranked as $Na^+ > Ca^{2+} > Mg^{2+} > K^+$, whereas the dominant anions followed the sequence of $HCO_3^- > NO_3^- > Cl^- > SO_4^{2-}$ (Fig. 2).

The $\delta^{18}O$ isotopic compositions across various aquifers were consistent, which was from −8.50‰ to −4.88‰, averaging at −6.26‰. And, the value of δ^2H ranged from

−58.0‰ to −28‰ with means of −39.50‰ in groundwater. Tritium of groundwater were from 0.1 TU to 3.6 TU, averaging at 1.74 TU. All samples contain detectable levels of tritium (0.1 TU).

3.2. Hydrochemical classification of groundwater

A Piper diagram was employed to classify the groundwater hydrochemical types with respect to nitrate concentrations. Three dominant hydrochemical types were identified: HCO_3-Ca, SO_4·Cl-Ca·Mg and Cl-Na (Fig. 3). Groundwater samples with low nitrate concentrations (<10 mg/L) predominantly exhibited the HCO_3-Ca. In contrast, samples with elevated nitrate levels (>50 mg/L) were classified as Cl-Na or SO_4 Cl-Ca·Mg.

Cations showed no statistically significant relationship with the nitrate concentration (left side of Fig. 3), whereas a noticeable shift in dominant anions from HCO_3^- to SO_4^{2-} and Cl^- was observed with increasing nitrate concentration (right side of Fig. 3). This transition indicated that elevated nitrate likely derived from anthropogenic sources, which introduced co-migrating anions (e.g., SO_4^{2-}, Cl^-) into the aquifer system,

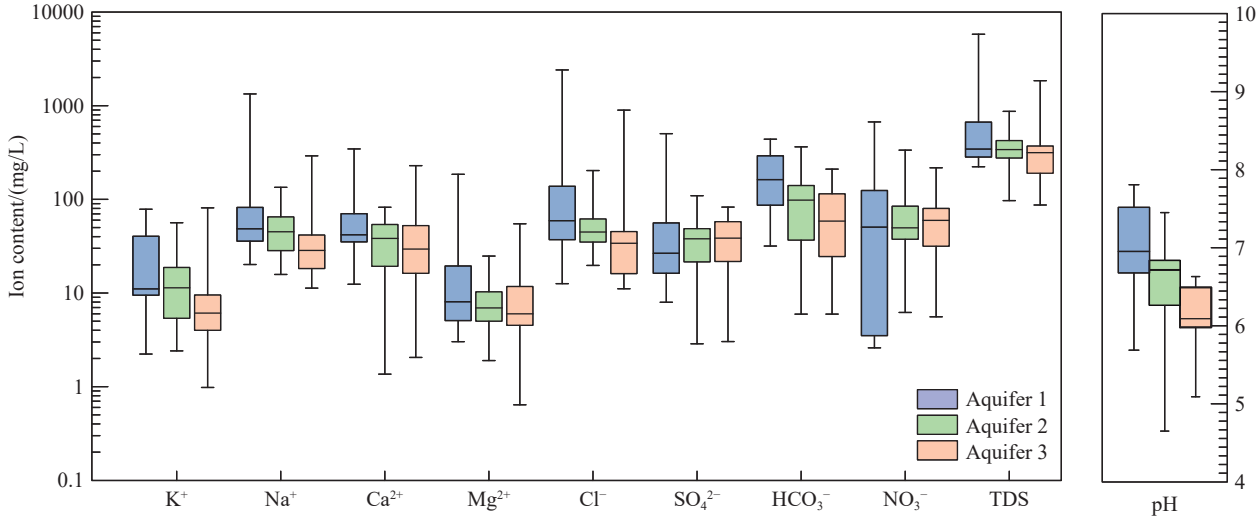


Fig. 2. Boxplots of various indices of the downstream Jinjiang Watershed.

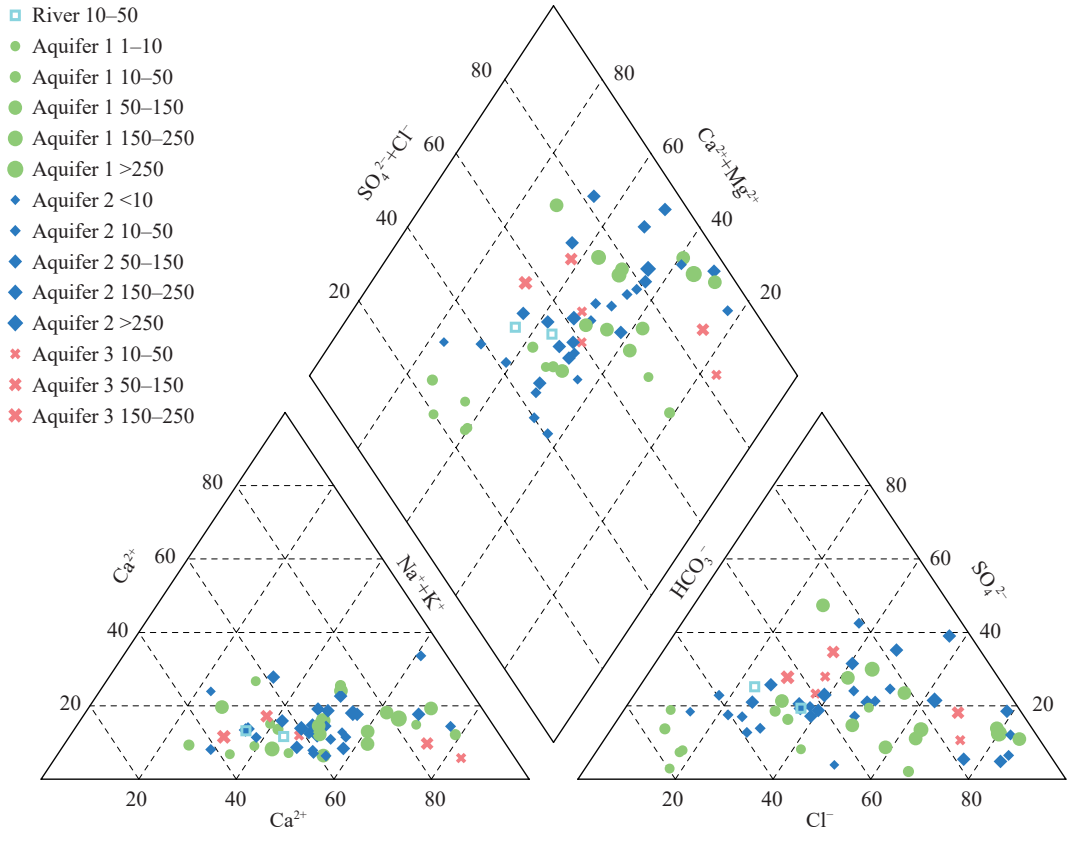


Fig. 3. Hydrochemical piper diagram of the groundwater with different concentrations of NO_3^-(mg/L) in the study area.

driving hydrochemical evolution toward saline facies (Luijendijk E et al., 2020).

Two surface water samples from Jinjiang and 99 Xi were identified as SO_4 Cl-Ca·Mg type, with low nitrate concentrations below 15 mg/L. Nevertheless, given that groundwater serves as a substantial recharge source for these surface waters, the samples are vulnerable to nitrate contamination.

3.3. Multivariate statistical analysis

Correlation analysis revealed significant positive associations between Cl^- and SO_4^{2-} (r = 0.89, p < 0.01) and between Cl^- and Ca^{2+} (r = 0.89, p < 0.01) (Table 1). Nitrate (NO_3^-) correlated strongly with Mg^{2+} (r = 0.78, p < 0.01) and Na^+ (r = 0.76, p < 0.01). PCA extracted two principal components (eigenvalues >1), collectively explaining 78.53% of the total variance (Table 2; Fig. 4a).

PC1 (58.2% variance) was heavily loaded with F^-, HCO_3^- and K^+ representing salinization processes. PC2 (20.3% variance) linked Cl^-, Mg^{2+}, NO_3^- and TDS, which is consistent with anthropogenic nitrate sources.

HCA (R-mode) grouped hydrochemical parameters into four clusters at a rescaled distance of 10 (Fig. 4b), aligning with the PCA factor loadings. (Fig. 4a). Cl^- exhibited a shorter distance for cluster rescaling (<2) with Na^+, Mg^{2+} and TDS, underscoring co-evolution during hydrochemical evolution. Conversely, NO_3^- formed a distinct cluster separate from K^+, HCO_3^-, F^- and pH, reflecting differential geochemical behaviour between nitrate-driven contamination and natural weathering processes.

4. Discussion

4.1. Isotopic constraints on groundwater recharge and flow mechanisms

Stable isotopes of deuterium (δ^2H) and oxygen ($\delta^{18}O$) provide critical insights into groundwater recharge dynamics and mixing processes. While, long-term local precipitation isotope data were unavailable for Quanzhou, the local meteoric water line (LMWL) derived from Fuzhou station ($\delta^2H = 8.19\delta^{18}O+11.81$; Chen ZY et al., 2010), which is situated approximately 150 km north of Quanzhou, was adopted as a regional proxy. Isotopic data for Fuzhou precipitation were obtained from the International Atomic Energy Agency (IAEA) Global Network of Isotopes of Precipitation (GNIP, 1986–1992). The volume-weighted annual mean and mean values for the $\delta^{18}O$ of precipitation in Fuzhou were –6.2‰ and –5.4‰, respectively (Chen ZY et al., 2010). The steeper slope of the LMWL relative to the global meteoric water line (GMWL, $\delta^2H = 8\delta^{18}O+10$), indicating higher humidity conditions during moisture recycling, consistent with coastal monsoonal regimes. During the sampling period (June), the $\delta^{18}O$ value of rain in Jinjiang region was –9.98‰, which was consistent with Fuzhou precipitation values ranging from –14.96‰ to –0.92‰.

The analytical results of the $\delta^{18}O$ and δ^2H values of the water samples were presented with LMWL and GMWL in Fig. 5. The distributions of $\delta^{18}O$ and δ^2H in groundwater exhibited scattered but closely aligned patterns with LMWL, confirming that atmospheric precipitation was the dominant recharge source. And, no notable differences were observed among the different groundwater flow systems.

However, two distinct groups (A and B) were visible in the δ^2H–$\delta^{18}O$ plot (Fig. 5a). Most groundwater samples plotted into Group B, tightly clustered around volume-weighted annual mean and mean modern precipitation values ($\delta^{18}O$: –6.2‰ and –5.4‰), slightly depleted relative to surface water samples ($\delta^{18}O$: –5.1‰ to –5.4‰, Fig. 5c) and slightly below and to the right of the LMWL. This suggested that groundwater was recharged mainly by rapid infiltration following local precipitation events, with minimal influence from evaporation during flow. Additionally, the groundwater samples generally trended parallel to the LMWL, supporting this conclusion. A few groundwater samples in Group A exhibited isotopically lighter values, implying recharge from heavy rainfall, high-elevation mountain precipitation, or rapid inflow.

The wide range of $\delta^{18}O$ (–8.50‰ to –4.81‰) and δ^2H (–58.0‰ to –28‰) values indicated that groundwater recharged from atmospheric precipitation with varied isotopic signatures and had not experienced significant evaporation fractionation. The results also suggested subtle differences in

Table 1. Correlations of hydrochemical parameters in groundwater.

Parameters	K^+	Na^+	Ca^{2+}	Mg^{2+}	Cl^-	SO_4^{2-}	HCO_3^-	NO_3^-	F^-	TDS	pH
K^+	1.00	0.61	0.76	0.63	0.65	0.61	0.57	0.45	–0.03	0.68	0.35
Na^+	0.61	1.00	0.85	0.98	0.98	0.93	0.53	0.76	–0.04	0.99	0.30
Ca^{2+}	0.76	0.85	1.00	0.89	0.89	0.83	0.60	0.69	–0.02	0.91	0.40
Mg^{2+}	0.63	0.98	0.89	1.00	0.98	0.92	0.51	0.78	–0.08	0.99	0.29
Cl^-	0.65	0.98	0.89	0.98	1.00	0.89	0.48	0.74	–0.08	0.99	0.26
SO_4^{2-}	0.61	0.93	0.83	0.92	0.89	1.00	0.53	0.75	–0.03	0.93	0.35
HCO_3^-	0.57	0.53	0.60	0.51	0.48	0.53	1.00	0.11	0.43	0.54	0.73
NO_3^-	0.45	0.76	0.69	0.78	0.74	0.75	0.11	1.00	–0.32	0.79	0.02
F^-	–0.03	–0.04	–0.02	–0.08	–0.08	–0.03	0.43	–0.32	1.00	–0.07	0.35
TDS	0.68	0.99	0.91	0.99	0.99	0.93	0.54	0.79	–0.07	1.00	0.32
pH	0.35	0.30	0.40	0.29	0.26	0.35	0.73	0.02	0.35	0.32	1.00

recharge seasons or path: (1) Recharge via direct precipitation in the locally unconfined system, the groundwater featured seasonal value of isotope from precipitation, and (2) recharged via isotopically depleted precipitation, these groundwater featured low value of isotope from precipitation. Despite these varying mechanisms, the range and average values of δ^2H and δ^{18}O across different groundwater aquifers were similar (Fig. 5). This uniformity suggested a consistent recharge area and hydrostratigraphy, with no significant isotopic different observed among the aquifers.

4.2. Dominant natural hydrogeochemical processes

4.2.1. Water-rock interactions

Groundwater flow conditions and geological environment jointly control the water-rock interactions of groundwater system. Groundwater in the western and central recharge zones predominantly exhibited HCO_3^- type, characterized by low NO_3^-(< 20 mg/L) and TDS (< 300 mg/L), reflecting rapid infiltration of precipitation (Section 4.1). Along the flow path toward the coastal fringe, the hydrochemical type transitioned to Cl^- (TDS >250 mg/L), reflecting modern SWI or residual effects of paleo-marine transgressions near coastal zones (Li J et al., 2017; Morici S et al., 2023). Additionally, the concentrations of major hydrochemical components generally increased along the groundwater flow direction (Fig. 2), typically from Aquifer 3 to Aquifer 1. Therefore, water-rock interactions, evaporation, and SWI were identified as primary hydrogeochemical processes.

Interactions of water-rock, specifically the hydrogeochemical leaching of rocks and minerals, were proved by over 90% of samples in the centre of the Gibbs diagram graph (Gibbs RJ, 1970; Marandi A and Shand P, 2018; Fig. 6). Oxidized hydrological environments are usually characterized by rapid, short distance flow, which enhances hydrogeochemical leaching processes. Elevated $[Na^+]/[Na^+ + Ca^{2+}]$ and $[Cl^-]/[Cl^- + HCO_3^-]$ ratios also corroborate dissolution of Na-rich silicates and carbonates (Gaillardet J et al., 1999; Chen JQ et al., 2023). What's more, for persistent effects of leaching insoluble carbonates and silicates were predominantly retained. The chemical composition of groundwater was characterized by these carbonates and silicates (Gaillardet J et al., 1999; Gao ZJ et al., 2021; Su H et al., 2023). Ion ratio plots (Fig. 7) also revealed that groundwater chemistry aligned closely with silicate endmembers, indicating that silicate rock weathering is the primary factor influencing the hydrogeochemical composition of groundwater in the DJW.

Groundwater hydrochemistry was also influenced to some extent by evaporation processes in the DJW area, as some groundwater samples were plotted in the upper-right quadrant of the Gibbs plots (Fig. 6). This phenomenon is likely exacerbated by the shallow water table depth (< 5 m) and capillary rise in coastal plain locations, where groundwater evaporation rates are relatively high (Han DM et al., 2014; Fu TF et al., 2022).

Critically, it was crucial to acknowledge that although most groundwater samples presented relatively high $[Na^+]/[Na^+ + Ca^{2+}]$ ratios, some samples showed relatively high $[Cl^-]/[Cl^- + HCO_3^-]$ ratios. Consequently, certain

Table 2. Principal component factor loading of groundwater chemical parameters.

Parameters	Factor 1	Factor 2
K^+	0.74	0.14
Na^+	0.97	–0.09
Ca^{2+}	0.94	0.03
Mg^{2+}	0.97	–0.13
Cl^-	0.96	–0.14
SO_4^{2-}	0.94	–0.05
HCO_3^-	0.62	0.70
NO_3^-	0.76	–0.48
F^-	–0.03	0.78
TDS	0.99	–0.10
pH	0.41	0.73
Eigenvalue	7.24	1.95
Explained variance/%	65.80	17.68
Cumulative of variance	65.80	83.48

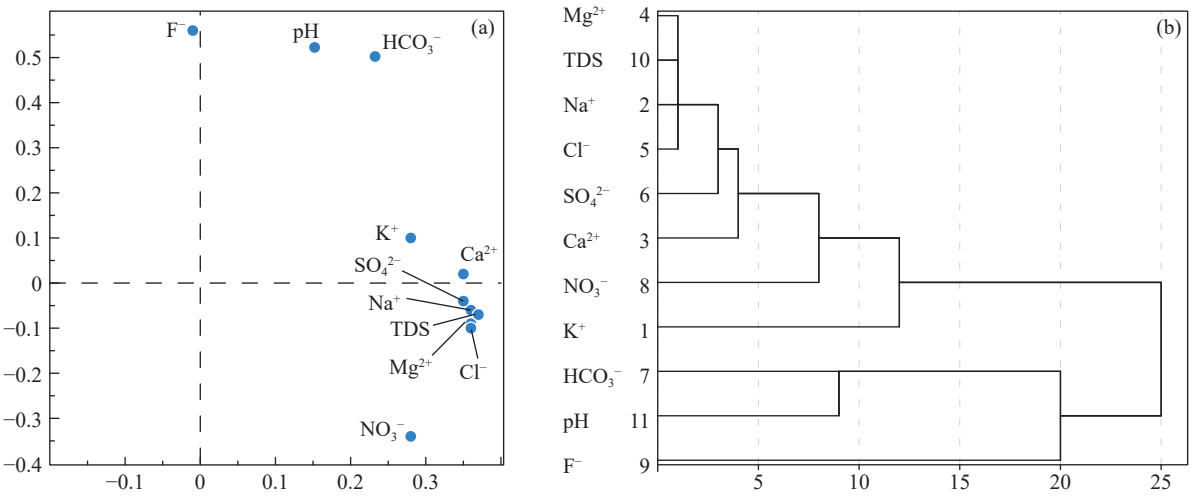


Fig. 4. a–Factor loadings of interrelationships among various indices; b–HCA dendrograms of chemical parameters.

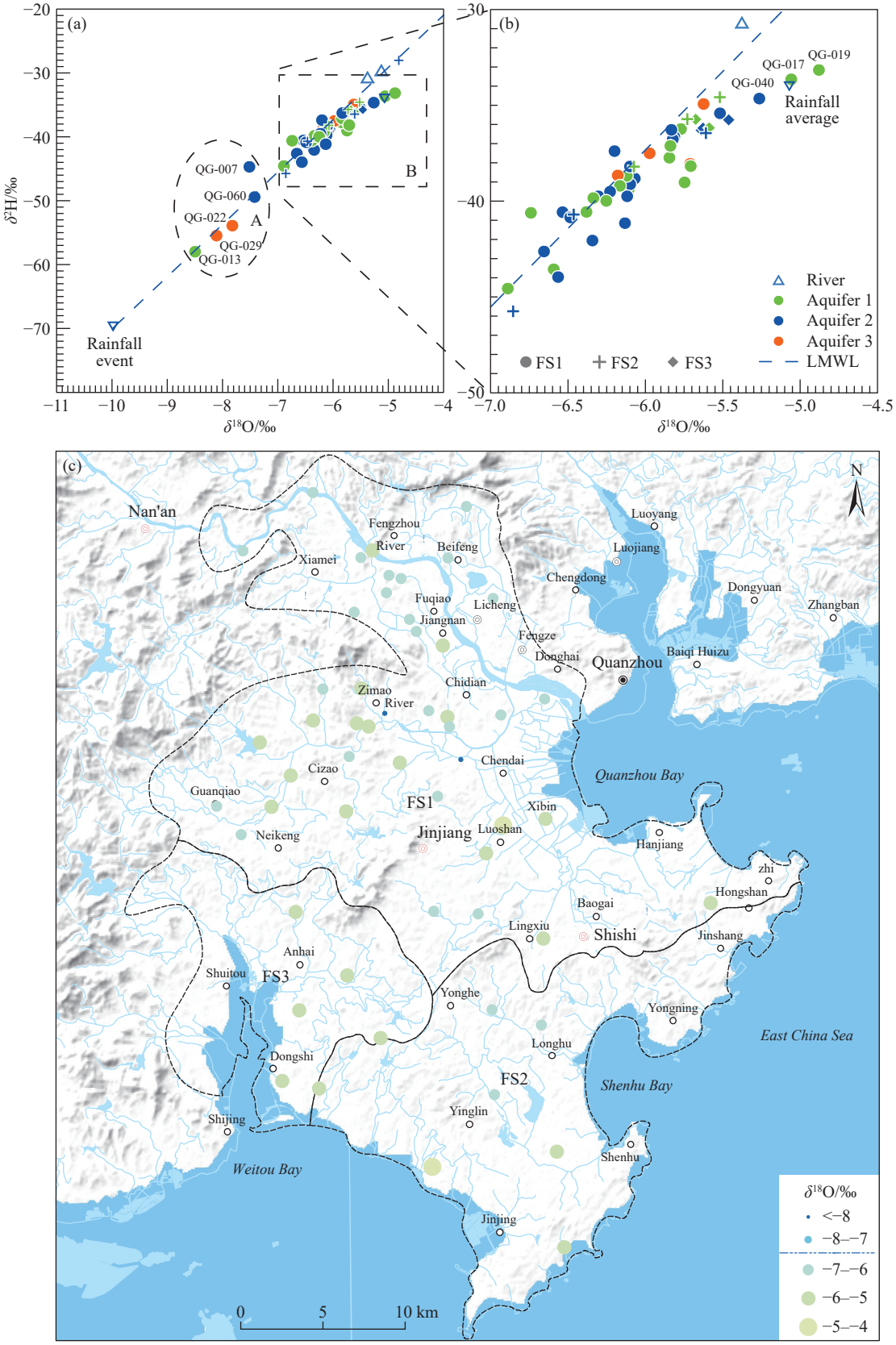


Fig. 5. a, b–Stable isotopic compositions of groundwater in the Jinjiang Downstream Watershed; c–spatial evolution of $\delta^{18}O$.

groundwater samples with elevated Na^+ and Cl^- ratios were positioned outside the water-rock interaction zone in the Gibbs diagram (Fig. 6), suggesting influence from other processes, such as cation exchange and SWI or contaminations influx from anthropogenic activities (Marandi A and Shand P, 2018; Wisitthammasri W et al., 2020; Ezzaouy Y et al., 2022).

To further elucidate the chemical processes and sources of

groundwater in the research area, a scatter diagram depicting various ions in groundwater was presented in Fig. 8. Most samples fell below the line $[Cl^-]/[Na^+]=1$ (Fig. 8a), reaffirming that the source of Na^+ and Cl^- was not solely from the dissolution of salt rocks (Chitsazan M et al., 2019; Chen JQ et al., 2023; Morici S et al., 2023). For the samples plotted below the [Cl]/[Na]=1 line the excess Na^+ was attributed to the leaching and dissolution of silicate minerals, such as Na-montmorillonite and Na-feldspar ($NaAlSi_3O_8 + H_2O + CO_2 \rightarrow Na^+ + HCO_3^- +$ kaolinite). Moreover, the concentration of Na^+ could also be influenced by cation exchange (Chitsazan M et al., 2019; Liu JT et al., 2024).

As illustrated in Fig. 8b, groundwater samples in the DJW primarily fell below the $[HCO_3^-+SO_4^{2-}]/[Ca^{2+}+Mg^{2+}]=1$ line, with a few samples marginally distributed on this line. This distribution further corroborated that leaching and dissolution of silicates constituted the major water-rock interaction in shaping the chemical composition of groundwater (Wisitthammasri W et al., 2020; Chen JQ et al., 2023).

4.2.2. Cation exchange

As mentioned above, cation exchange might be another

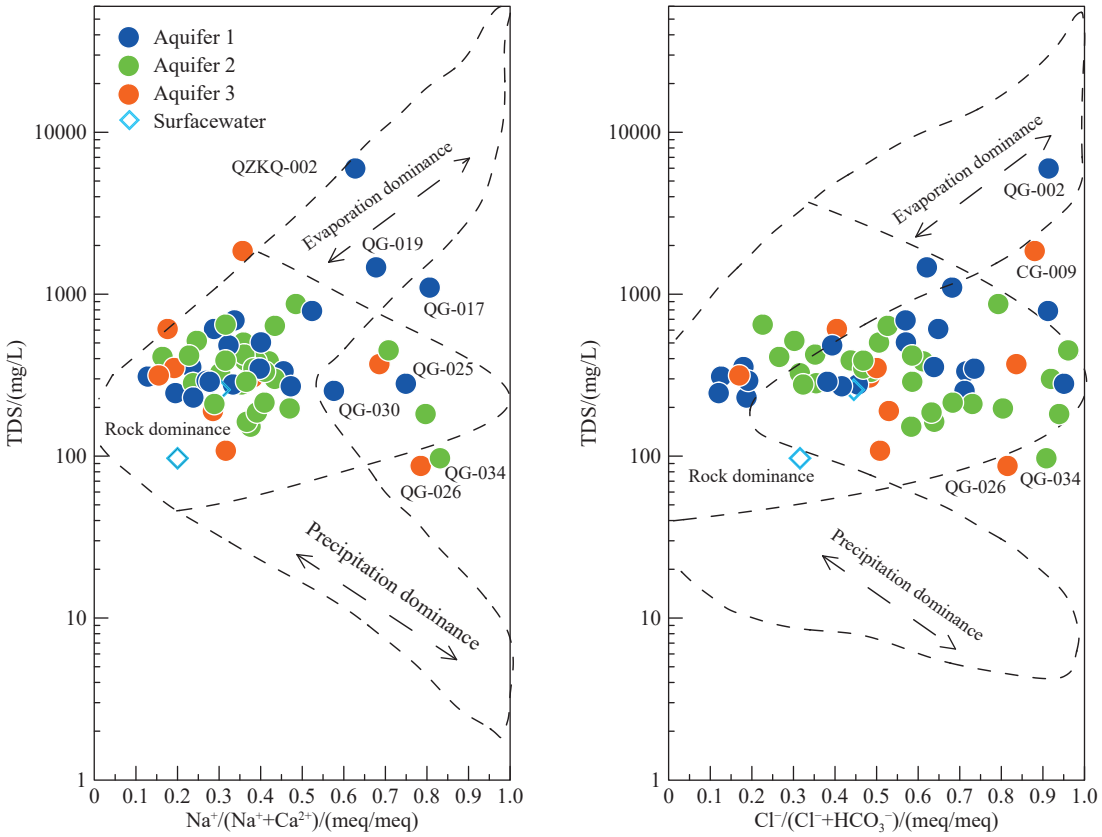


Fig. 6. Gibbs plots of the major ions in the groundwater in the DJW.

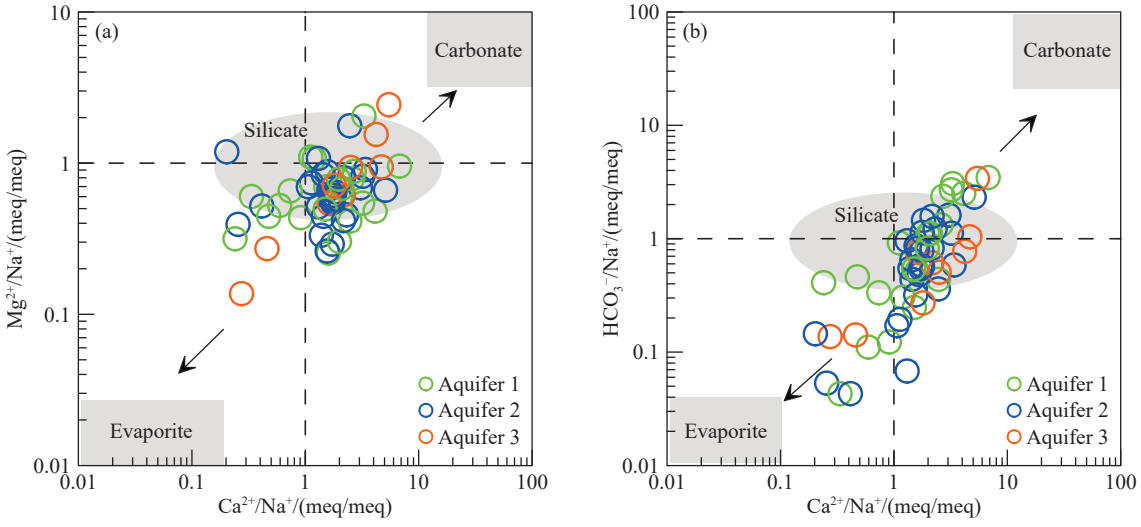


Fig. 7. Mixing diagrams of Ca^{2+}/Na^+ *vs.* Mg^{2+}/Na^+ (a) and Ca^{2+}/Na^+ *vs.* HCO_3^-/Na^+ (b) explaining the geochemical processes in groundwater.

driving force effecting hydrochemistry. The $(Ca^{2+}+Mg^{2+})-(HCO_3^-+SO_4^{2-})$ *vs.* $(Na^++K^+)-Cl^-$ plot clearly showed that most of groundwater samples were plotted near the −1 line and in the upper right quadrant (Fig. 9a). It dominated that Ca^{2+} adsorption onto clay surfaces releases Na^+ into solution, indicating a positive cation exchange reaction ($Ca^{2+} + 2Na_{clay} \rightarrow 2Na^+ + Ca_{clay}$) (Wang H et al., 2021; Su H et al., 2023). This process explains Na^+–HCO_3^- facies in recharge zones. The relationship between the two Chlor-alkali indices in Fig. 9b also indicated that the predominance of positive cation exchange in the groundwater of the DJW (Fu CC et al., 2018; Wisitthammasri W et al., 2020).

4.3. Seawater intrusion

Seawater intrusion (SWI) is a critical environmental challenge in coastal areas and occurs when the chloride (Cl) concentration in groundwater exceeds 250 mg/L or the TDS exceeds 1000 mg/L. SWI severity is categorized into four levels: No intrusion (<250 mg/L Cl), mild (250–500 mg/L Cl), moderate (500–1000 mg/L Cl), and severe (>1000 mg/L Cl) (Zhang B et al., 2013; Liu JT et al., 2024). Except for a few outliers, such as samples QG-002 (2486 mg/L), QG-017 (442.3 mg/L), QG-019 (430.8 mg/L), QG-033 (331.3 mg/L), and CG-009 (896.3 mg/L), most samples (about 86%) had Cl concentrations less than 250 mg/L (Fig. 10). Spatially, high-Cl^- samples clustered within 1.5 km of the coastline (Fig. 1), aligning with recent SWI surveys in Fujian Province reporting intrusion plumes extending up to 3.9 km inland (Han DM and Currell MJ, 2022).

The evolution of coastal aquifer salinity can be effectively depicted via a multi rectangular hydrochemical facies evolution diagram (HFE-D) (Giménez-Forcada E, 2014). This method considers major ion percentages, and visually illustrated phases of SWI and freshening in hydrochemical facies. In the Fig. 10, most samples were plotted within the freshwater and seawater mixing field (CML) of the HFE-D. Samples on the right of the CML means mixture of freshwater and seawater components with Na-Ca inverse cation exchange predominates. Approximately 66.1% samples plotted within

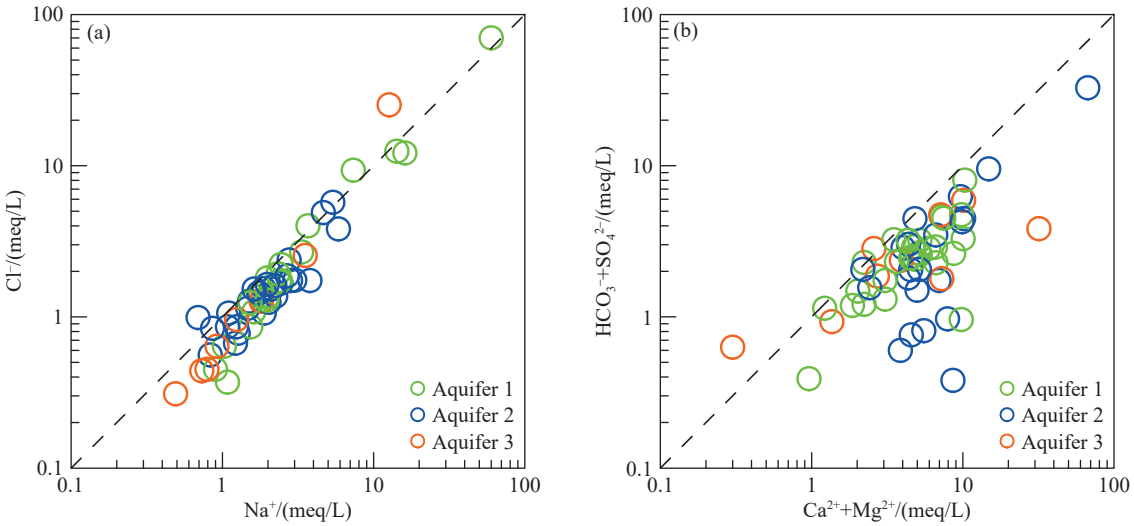


Fig. 8. Scatter plots of the main ion ratios in groundwater.

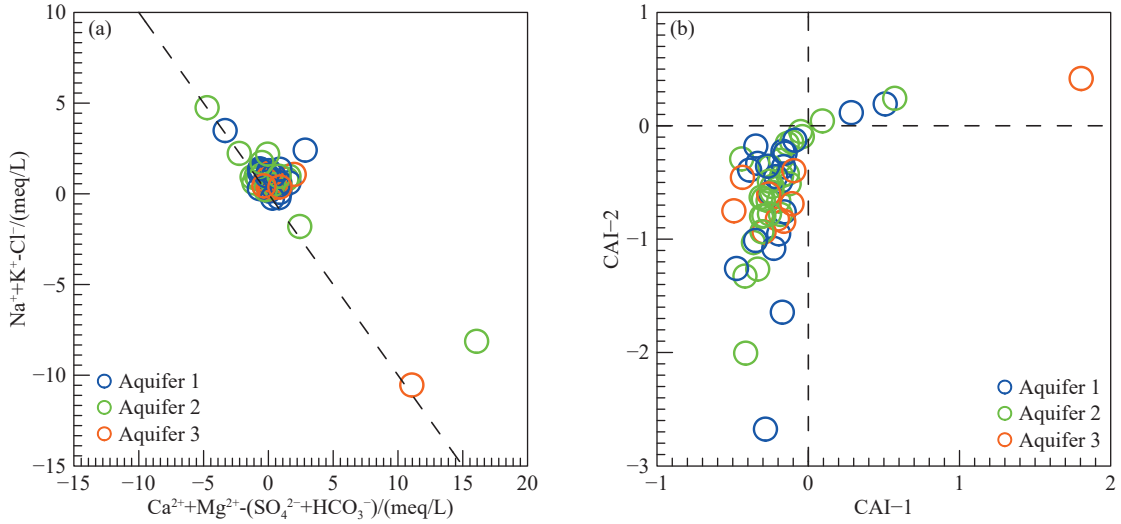


Fig. 9. Diagrams of the relationship of $[(Ca^{2+}+Mg^{2+})-(HCO_3^-+SO_4^{2-})]$*vs.*$[(Na^++K^+)-Cl^-]$ (a) and CAI−1 *vs.* CAI−2 (b) in groundwater.

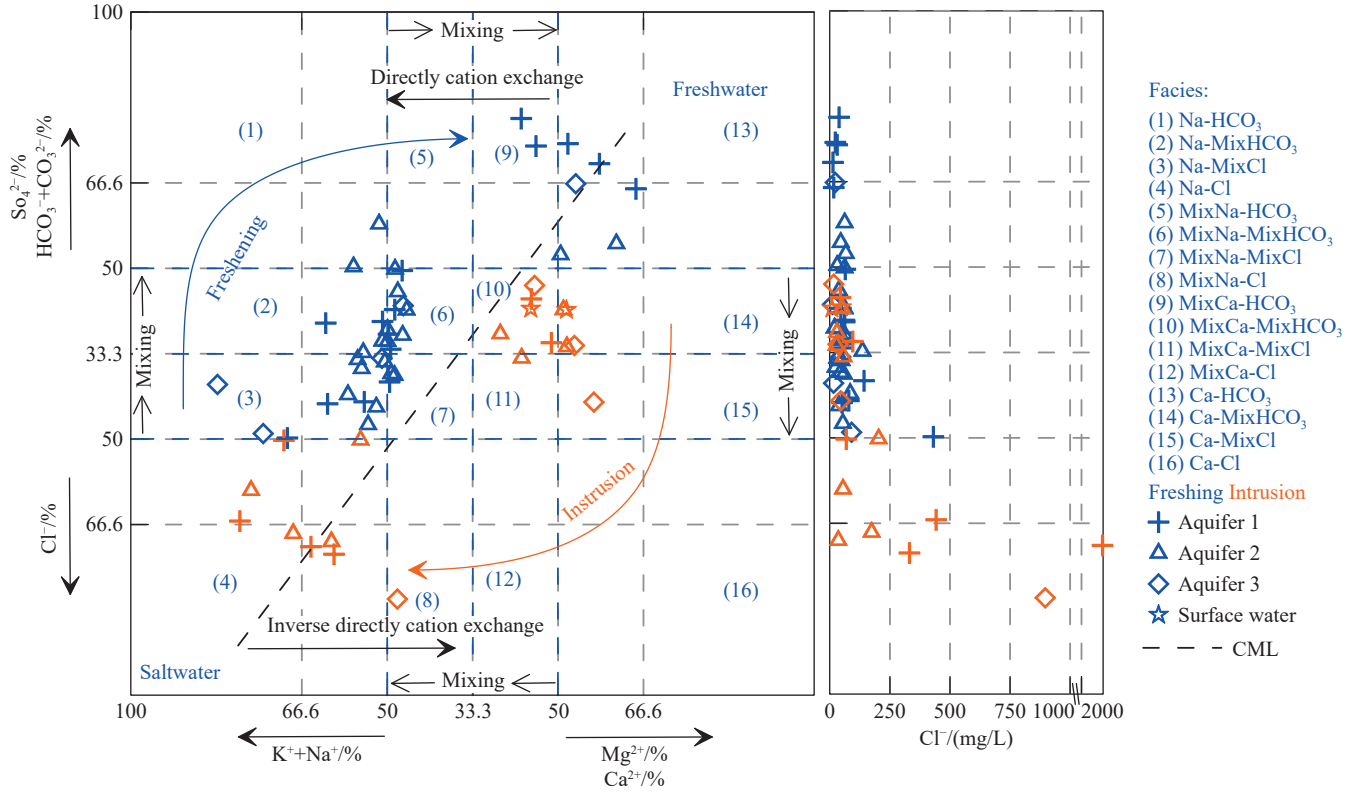


Fig. 10. Hydrochemical facies evolution (HFE) diagram, showing all water samples in relation to the intrusion and freshening substages, and the CML. On the right, the samples are represented in terms of their Cl^- values (after Giménez-Forcada E et al., 2014).

the freshening field, which were characterized by Ca-HCO_3 facies. While 33.9% samples occupied the intrusion zone with notable Na-Ca reverse ion exchange (Fig. 10). Notably, discrepancies between hydrochemical facies and TDS values were observed: Samples in intrusion phase displayed a typically low TDS. This anomaly may result from rapid infiltration of low-salinity precipitation overriding seawater contributions typical in coastal areas (Liu Y et al., 2017; Rogers KM et al., 2023). For example, sample QG-034 belonged to the Na-Cl facies, but its TDS was 35.1 mg/L with detectable levels of ^{3}H. They underscore the rapid recharge regimes from monsoon precipitation and transient nature of freshwater-seawater interfaces under modern sea intrusion regimes (Santoni S et al., 2018).

The hydrochemical and isotopic signatures of groundwater in the DJW provide critical insights into the temporal and spatial dynamics of SWI. While Quanzhou Bay in the study area experienced marine sedimentary environments in its geological past, as evidenced by stratigraphic records of Holocene transgression events and preserved marine clay layers (Wu CC et al., 2011; Zhao HM et al., 2023). Groundwater samples within Quanzhou Bay, predominantly collected from shallow aquifers (<20 m depth), exhibit detectable levels of tritium (^{3}H) with activities ranging from 0.1 TU to 2.2 TU. These values align with the temporal decay profile of ^{3}H in local precipitation since the 1960s, confirming that recharge originates predominantly from post-1960 precipitation and effectively precluding contributions from ancient seawater or connate brine (Han DM et al., 2011; Clark ID and Fritz P, 2013). Therefore, contemporary salinity anomalies are unequivocally linked to modern hydrological processes rather than paleo-saline water remnants.

Oxygen isotope (δ^{18}O) analysis further refined this interpretation. Groundwater samples from near Quanzhou Bay were enriched in δ^{18}O by 1.5‰–2.0‰ relative to inland samples (Fig. 5c), a signature consistent with modern seawater mixing rather than legacy saline reservoirs (Carretero S et al., 2022; Craig H, 1961). This enrichment trend correlates spatially with elevated chloride concentrations (>250 mg/L) in coastal wells. The consistency between ^{3}H-derived modern recharge ages, δ^{18}O enrichment, and Cl^- anomalies underscored that salinity incursions are driven by contemporary SWI, rather than paleo-hydrogeological processes.

Collectively, these findings demonstrate that while SWI is an active process in the study area, its magnitude is constrained relative to that of other coastal systems documented globally. The dominant hydrogeochemical evolution appears to be driven by silicate weathering and carbonate dissolution along flow paths, as evidenced by the prevalence of Ca-HCO_3 water (Fig. 10). Nevertheless, rising sea levels and anthropogenic groundwater extraction may exacerbate intrusion risks, necessitating adaptive monitoring strategies.

4.4. Origins and driving forces for nitrate in groundwater

Despite limited SWI, the groundwater exhibited severe

nitrate contamination, with concentrations exceeding China's groundwater quality standard (>20 mg/L N). A variety of nitrogen-rich human activities, such as agricultural fertilizers, animal husbandry waste, industrial wastewater and landfills, domestic sewage and septic tanks can result in elevated NO_3^- levels (Matiatos I et al., 2021; Zhang H Yet al., 2023; Wang D et al., 2024).

The relationship between NO_3^- and Cl^- concentrations is commonly utilized to distinguish the sources of nitrate pollutants. Recent studies have highlighted a positive correlation between NO_3^- and Cl^- concentrations in domestic sewage or landfill leachate, particularly in rural settlements lacking centralized wastewater infrastructure (Ez-zaouy Y et al., 2022; Liu RN et al., 2024). A moderate to strong positive correlation was observed between NO_3^- and Cl^- concentrations in groundwater samples, particularly within the high NO_3^- group (Table 2; Fig.11a). This indicated that domestic sewage was the primary source of NO_3^- in DJW.

The use of nitrogen-bearing fertilizers elevates the NO_3^- concentration without a corresponding increase in Cl^- concentration, resulting in a higher $[NO_3^-]/[Cl^-]$ ratio in agricultural regions than other areas (Rogers KM et al., 2023; Wang SQ et al., 2024). The ratio serves as a crucial indicator for distinguishing NO_3^- sources. According to Fig. 11b, the high-NO_3^- samples did not presented high $[NO_3^-]/[Cl^-]$ ratios, suggesting that fertilizers were not a significant NO_3^- source in the research area. Conversely, septic tank leakage infiltrated into the groundwater, resulting in elevated Cl^- concentrations in the research region.

Moreover, NO_3^- concentrations exceeding 50 mg/L were predominantly found in rural residential areas with impermeable land use types (Fig. 12), where the discharge of untreated domestic sewage was prevalent due to inadequate sewage infrastructure in residential zones.

The concentration of NO_3^- in groundwater sample CG-010 notably reached 79.89 mg/L with well depth of 100 m. This observation indicated rapid contaminant transport via fracture networks in slope pore-fissure rocks and fissure aquifers (Khan MR et al., 2016). Such pathways bypass natural attenuation in clay layers, highlighting the vulnerability of deep groundwater to anthropogenic pollutants—a growing concern in fractured coastal systems. The ^3H activity of sample CG-010 (1.8 TU) was consistent with the ^3H activity (1.1 TU) of the rain collected during the sampled period, aligned with modern recharge and further supported this phenomenon.

The results for surface water (13.99–14.17 mg/L NO_3^-) differed notably from those for groundwater. This divergence arises from coupled hydrogeochemical and anthropogenic processes. In the Jinjiang River, high discharge rates (5.3×10^9 m^3/yr) drive rapid dilution of nitrate inputs, particularly downstream of urban centers where NO_3^- concentrations remain below 7 mg/L. The occurrence of monsoon-driven rainwater influx, accounting for >82% of this dilution (Zhu YC et al., 2024), is corroborated by enriched $\delta^{18}O$-H_2O values (−5.4‰ to −5.1‰) in surface water samples during the monsoon season. This transient dilution masks acute rural residential pollution but fails to mitigate long-term aquifer contamination. Groundwater, in contrast, integrates cumulative nitrate loads over several decades.

The difference in nitrogen dynamics between groundwater and surfacer systems also lead to nitrate enrichment in groundwater. During wet seasons, surface water recharge accelerates NH_4^+ release from sediments through desorption mechanisms, triggering nitrification reactions that elevate groundwater NO_3^- concentrations (Yang Y et al., 2024). In contrast, dry season groundwater discharge reduces NH_4^+ mobility by enhancing adsorption onto sedimentary matrices, consequently lowering surface water nitrate levels (Zhang AG et al., 2024). Moreover, river hyporheic zones facilitate nitrogen transformation through variable redox conditions driven by water table fluctuations, enhancing both nitrification and denitrification (Peng C et al., 2024).

The multivariate statistical techniques PCA and HCA were employed to further analyse the NO_3^- sources in the study area. Factor 1 of the PCA exhibited strong positive

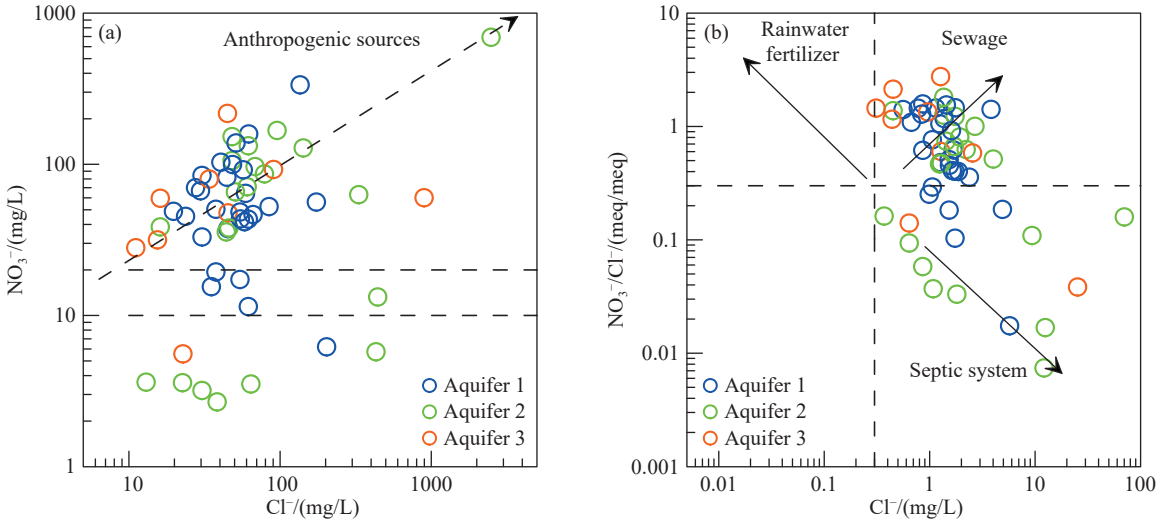


Fig. 11. Relationships of $[NO_3^-]$ *vs.* $[Cl^-]$ and $[NO_3^-]/[Cl^-]$ *vs.* $[Cl^-]$ in groundwater.

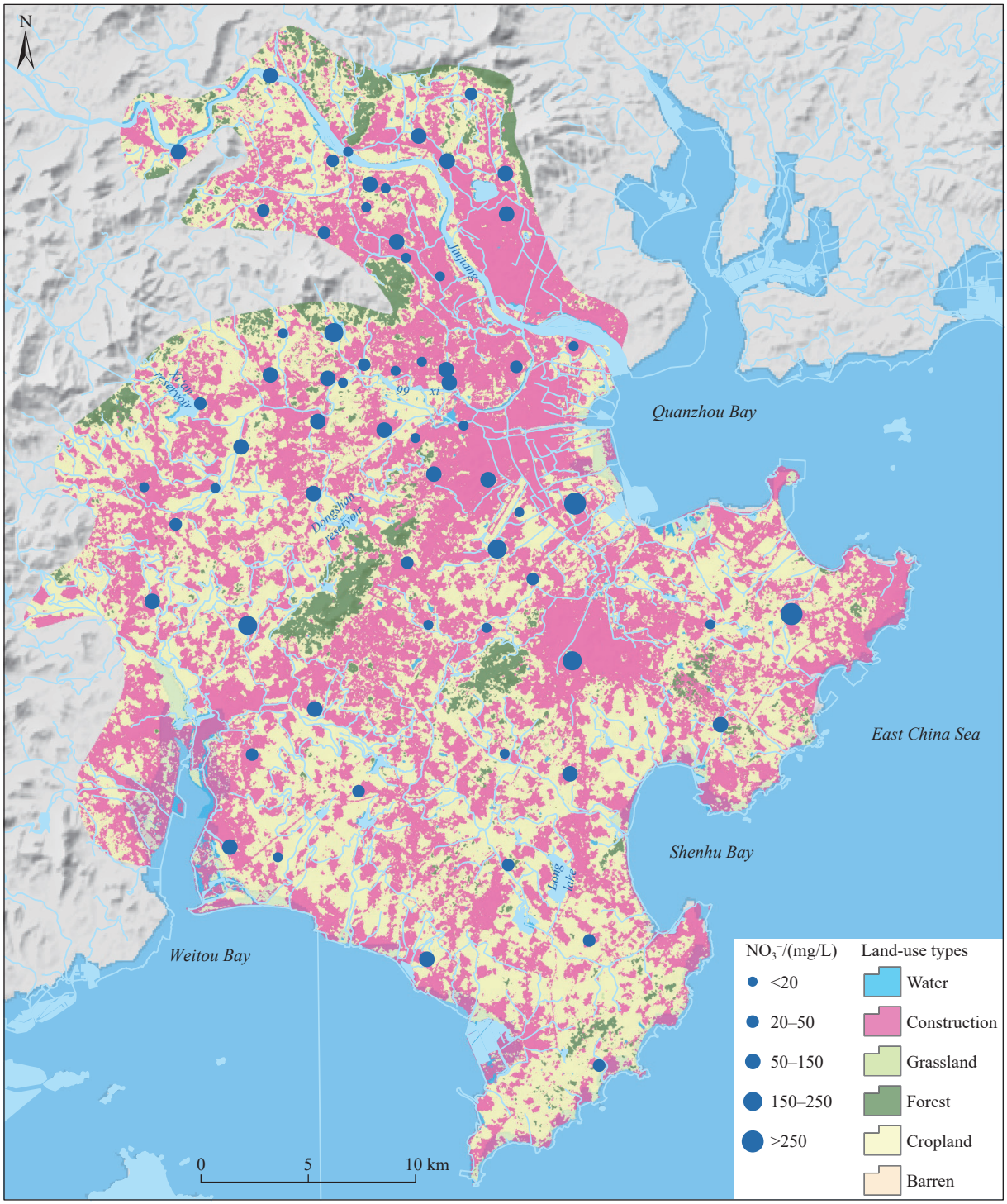


Fig. 12. Land use types and spatial distributions of nitrate concentrations.

loadings for Na^+, Mg^{2+} and Cl^- and moderate positive loadings for NO_3^- (Table 1). Previous studies have established that the co-occurrence of NO_3^-, Cl^-, and Na^+ in principal components typically indicates anthropogenic inputs originating from septic systems, human faeces, and animal manure (Su C et al., 2020; Zhang M et al., 2020; Liu RN et al., 2024). This factor therefore serves as a reliable indicator of human-induced contamination pathways in groundwater systems. The HCA results corroborated the PCA-derived interpretation, revealing a clear clustering pattern where NO_3^- formed a tight association with Cl^- and Na^+, and was distinctly separated from the F^- dominated group (Fig. 4b). Such disparate clustering patterns support the distinction between anthropogenic and natural nitrogen sources, as fluoride ions are associated primarily with geogenic processes in carbonate aquifers.

4.5. Indication for regional groundwater protection

The sustainability of coastal aquifers in Southeast China

depends on balancing anthropogenic demands with ecological preservation. The slope pore-fissure aquifers of the DJW, characterized by limited thickness, low specific yield and anisotropic flow, are recharged primarily by seasonal precipitation, rendering them susceptible to both SWI and nitrate contamination. While SWI remains spatially constrained, the synergy between modern recharge pathways and anthropogenic nitrate loading creates compounded risks. Furthermore, these aquifers act as both cumulative sink for basin-scale pollutants in groundwater and a rapid conveyor of surface-derived contaminants.

This dual contamination pattern underscores the need for coordinated groundwater-surface water monitoring. Along agricultural-urban transition belts, where nitrate concentrations correlate strongly with septic system density, high-frequency electrochemical sensor networks for NO_3^-/Cl^- could capture sub-daily pollution pulses inherent to thin aquifers and offering unprecedented capacity to map contamination hotspots (Kurwadkar S et al., 2020; Liu Y et al., 2022).

At the critical freshwater-seawater interface, predictive management requires merging physical sensing with machine intelligence. Nearshore submarine discharge arrays integrating radon-222 detectors and electrochemical Cl^- sensors could feed data into LSTM neural networks trained to recognize electrical conductivity-chloride hysteresis patterns (Wang ZY et al., 2023; Zheng R et al., 2024). Such systems can provide early warnings of salinity thresholds, which when coupled with phased septic system upgrades to membrane bioreactor (MBR) plants (could lower nitrate export coefficients 3.9–12.7kg-N/ha/yr), directly advance SDG 6 targets.

Ultimately, protecting these aquifers necessitates converting hydrochemical insights into adaptive engineering. This tiered approach —bridging process science with smart infrastructure —offers a replicable framework to reconcile coastal groundwater security with escalating anthropogenic and climatic pressures.

5. Conclusion

Coastal groundwater systems, functioning as critical buffers between terrestrial ecosystems and marine environments, face escalating pressures from both natural hydrodynamics and intensifying human activities, hindering the achievement of SDG related to water security and ecosystem health. Their dual role in sustaining freshwater supplies and mitigating SWI underscores the urgent need to unravel hydrochemical driving forces —a prerequisite for achieving water security in rapidly urbanizing coastal zones. Here, hydrogeological vulnerabilities to contamination and salinization are amplified by thin aquifers and short groundwater flow paths.

This study advances coastal groundwater science through three key revelations. The aquifer's hydrochemical architecture, shaped by topography-driven flow regimes, demonstrates a systematic transition from HCO_3^- dominated recharge zones to Cl^- enriched discharge areas, governed by the synergistic interplay of silicate mineral dissolution, seawater mixing, and anthropogenic forcing. Isotopic fingerprints (δ^2H, $\delta^{18}O$) and detectable levels of ^3H confirm modern precipitation as the dominant recharge source, and fracture networks in slope pore-fissure and fissure aquifers enable rapid nitrate migration to deeper zones. While current SWI impacts remain spatially constrained, the synergy between unregulated sewage discharge, preferential contaminant pathways, and modern recharge dynamics poses escalating threats.

These findings recommend a governance paradigm shift integrating technological innovation with hydrogeochemical resilience. A tiered management framework should prioritize: (1) Deployment of electrochemical sensor networks for real-time NO_3^-/Cl^- monitoring, coupled with machine learning algorithms to predict contaminant pathways through fractured media; (2) phased replacement of septic systems with membrane bioreactor treatment plants in high-density rural district clusters. Implementing this strategy could reduce nitrate fluxes while preserving the aquifer's freshening trajectory, offering a transferable model for SDG-aligned coastal groundwater management in climate-vulnerable regions.

CRediT authorship contribution statement

Zhong-shuang Cheng contributed to original draft writing, methodology, and data curation. Chen Su contributed to methodology, investigation, and resources. Wen-zhong Wang contributed to resources and funding acquisition. Bing-yan Li, En-de Zuo, and Yu-meng Tian contributed to investigations and figures. Zhao-xian Zheng contributed to supervision and conceptualization. All authors discussed the results and contributed to the final manuscript.

Declaration of competing interest

The authors declare no conflicts of interest.

Acknowledgement

This work was supported by the project of the China Geological Survey (DD20230421), the Central Institutes Fundamental Research Project (SK202410) and the National Natural Science Foundation of China (41702283).

References

Amiri V, Sohrabi N, Li PY, Amiri F. 2023. Groundwater quality for drinking and non-carcinogenic risk of nitrate in urban and rural areas of Fereidan, Iran. Exposure and Health, 15(4), 807–823. doi: 10.1007/s12403-022-00525-w.

Anaman R, Peng C, Jiang ZC, Liu X, Zhou ZR, Guo ZH, Xiao XY. 2022. Identifying sources and transport routes of heavy metals in soil with different land uses around a smelting site by GIS based PCA and PMF. Science of the Total Environment, 823, 153759. doi: 10.1016/j.scitotenv.2022.153759.

Carretero S, Rodrigues Capítulo L, Dapeña C, Fabiano M, Kruse E. 2022. A chemical and isotopic approach to investigate groundwater dynamics in a coastal aquifer. Catena, 213, 106229. doi: 10.1016/j.catena.2022.106229.

Chen JQ, Yan BZ, Xu TB, Xia F. 2023. Hydrochemical evolution characteristics and mechanism of groundwater funnel areas under artificial governance in Hengshui City, North China. Ecological Indicators, 148, 110059. doi: 10.1016/j.ecolind.2023.110059.

Chen ZY, Qi JX, Zhang ZJ. 2010. Application of Isotope Hydrogeology Method in Typical Basins of North China. Beijing, Science Press, 24–25 (in Chinese).

Cheng ZS, Su C, Zheng ZZ, Li Z, Wang LK, Wang EB. 2021. Grain size characteristics and genesis of the Muxing loess in the Muling-Xingkai Plain, Northeast China. Journal of Groundwater Science and Engineering, 9(2), 152–160. doi: 10.19637/j.cnki.2305-7068.2021.02.007.

Chitsazan M, Aghazadeh N, Mirzaee Y, Golestan Y. 2019. Hydrochemical characteristics and the impact of anthropogenic activity on groundwater quality in suburban area of Urmia city, Iran. Environment, Development and Sustainability, 21(1), 331–351. doi: 10.1007/s10668-017-0039-1.

Clark ID, Fritz P. 2013. Environmental Isotopes in Hydrogeology. Boca Raton, CRC Press, 174–176.

Craig H. 1961. Isotopic variations in meteoric waters. Science, 133(3465), 1702–1703. doi: 10.1126/science.133.3465.1702.

Egbueri JC. 2020. Groundwater quality assessment using pollution index of groundwater (PIG), ecological risk index (ERI) and hierarchical cluster analysis (HCA): A case study. Groundwater for Sustainable Development, 10, 100292. doi: 10.1016/j.gsd.2019.100292.

Ez-zaouy Y, Bouchaou L, Saad A, Hssaisoune M, Brouziyne Y, Dhiba D, Chehbouni A. 2022. Morocco's coastal aquifers: Recent observations, evolution and perspectives towards sustainability. Environmental Pollution, 293, 118498. doi: 10.1016/j.envpol.2021.118498.

Fu CC, Li XQ, Ma JF, Liu LX, Gao M, Bai ZX. 2018. A hydrochemistry and multi-isotopic study of groundwater origin and hydrochemical evolution in the middle reaches of the Kuye River basin. Applied Geochemistry, 98, 82–93. doi: 10.1016/j.apgeochem.2018.08.030.

Fu TF, Qi C, Wang ZY, Li CZ, Liu WQ, Fu YS, Chen GQ, Su Q, Xu XY, Yu HJ. 2022. Hydrochemical characteristics and quality assessment of groundwater under the impact of seawater intrusion and anthropogenic activity in the coastal areas of Zhejiang and Fujian Provinces, China. Lithosphere, 2022, 1394857. doi: 10.2113/2022/1394857.

Gaillardet J, Dupré B, Louvat P, Allègre CJ. 1999. Global silicate weathering and CO_2 consumption rates deduced from the chemistry of large rivers. Chemical Geology, 159(1–4), 3–30. doi: 10.1016/S0009-2541(99)00031-5.

Gao ZJ, Han C, Xu Y, Zhao ZH, Luo ZJ, Liu JT. 2021. Assessment of the water quality of groundwater in Bohai Rim and the controlling factors—a case study of northern Shandong Peninsula, north China. Environmental Pollution, 285, 117482. doi: 10.1016/j.envpol.2021.117482.

Gibbs RJ. 1970. Mechanisms controlling world water chemistry. Science, 170(3962), 1088–1090. doi: 10.1126/science.170.3962.1088.

Giménez-Forcada E. 2014. Space/time development of seawater intrusion: A study case in Vinaroz coastal plain (Eastern Spain) using HFE-Diagram, and spatial distribution of hydrochemical facies. Journal of Hydrology, 517, 617–627. doi: 10.1016/j.jhydrol.2014.05.056.

Han DM, Kohfahl C, Song XF, Xiao GQ, Yang JL. 2011. Geochemical and isotopic evidence for palaeo-seawater intrusion into the south coast aquifer of Laizhou Bay, China. Applied Geochemistry, 26(5), 863–883. doi: 10.1016/j.apgeochem.2011.02.007.

Han DM, Currell MJ. 2022. Review of drivers and threats to coastal groundwater quality in China. Science of the Total Environment, 806, 150913. doi: 10.1016/j.scitotenv.2021.150913.

Han DM, Song XF, Currell MJ, Yang JL, Xiao GQ. 2014. Chemical and isotopic constraints on evolution of groundwater salinization in the coastal plain aquifer of Laizhou Bay, China. Journal of Hydrology, 508, 12–27. doi: 10.1016/j.jhydrol.2013.10.040.

Han DM, Song XF, Currell MJ. 2016. Identification of anthropogenic and natural inputs of sulfate into a karstic coastal groundwater system in northeast China: Evidence from major ions, δ^{13}C-DIC and δ^{34}S-SO_4. Hydrology and Earth System Sciences, 20(5), 1983–1999. doi: 10.5194/hess-20-1983-2016.

Hou QX, Zhang Q, Huang GX, Liu CY, Zhang Y. 2020. Elevated manganese concentrations in shallow groundwater of various aquifers in a rapidly urbanized delta, south China. Science of The Total Environment, 701, 134777. doi: 10.1016/j.scitotenv.2019.134777.

Huang GX, Li LP. 2024. Groundwater Chemistry and Quality in Coastal Aquifers. Water, 16(14), 2041. doi: 10.3390/w16142041,.

Huang GX, Liu CY, Sun JC, Zhang M, Jing JH, Li LP. 2018. A regional scale investigation on factors controlling the groundwater chemistry of various aquifers in a rapidly urbanized area: A case study of the Pearl River Delta. Science of The Total Environment, 625, 510–518. doi: 10.1016/j.scitotenv.2017.12.322.

Khan MR, Koneshloo M, Knappett PSK, Ahmed KM, Bostick BC, Mailloux BJ, Mozumder RH, Zahid A, Harvey CF, van Geen A, Michael HA. 2016. Megacity pumping and preferential flow threaten groundwater quality. Nature Communications, 7(1), 12833. doi: 10.1038/ncomms12833.

Kurwadkar S, Kanel SR, Nakarmi A. 2020. Groundwater pollution: Occurrence, detection, and remediation of organic and inorganic pollutants. Water Environment Research, 92(10), 1659–1668. doi: 10.1002/wer.1415,.

Kwon HI, Koh DC, Cho BW, Jung YY. 2022. Nutrient dynamics in stream water and groundwater in riparian zones of a mesoscale agricultural catchment with intense seasonal pumping. Agricultural Water Management, 261, 107336. doi: 10.1016/j.agwat.2021.107336.

Li CC, Gao XB, Li SQ, Bundschuh J. 2020. A review of the distribution, sources, genesis, and environmental concerns of salinity in groundwater. Environmental Science and Pollution Research, 27(33), 41157–41174. doi: 10.1007/s11356-020-10354-6.

Li BJ, Liang X, Jin MG, Yang JL, Ma B, Ge Q. 2017. Origin and evolution of aquitard porewater in the western coastal plain of Bohai Bay, China. Groundwater, 55(6), 917–925. doi: 10.1111/gwat.12590.

Li ZH, Li JF, Huang JO, Li YS. 2024. Nitrate contamination in groundwater and its health risk assessment: A case study of Quanzhou, a typical coastal city in Southeast China. Environmental Earth Sciences, 83(10), 331. doi: 10.1007/s12665-024-11608-z.

Lin L, Pussella P. 2017. Assessment of vulnerability for coastal erosion with GIS and AHP techniques case study: Southern coastline of Sri Lanka. Natural Resource Modeling, 30(4), e12146. doi: 10.1111/nrm.12146.

Lingle DA, Kehew AE, Krishnamurthy RV. 2017. Use of nitrogen isotopes and other geochemical tools to evaluate the source of ammonium in a confined glacial drift aquifer, Ottawa County, Michigan, USA. Applied Geochemistry, 78, 334–342. doi: 10.1016/j.apgeochem.2017.01.004.

Liu CL, Zheng JH, Li ZH, Li YS, Hao QC, Li JF. 2021. Analysis on the situation and countermeasures of water resources supply and demand in the cities of small and medium-sized river basins along southeast coast of China —taking Xiamen City as an example. Journal of Groundwater Science and Engineering, 9(4), 350–358. doi: 10.19637/j.cnki.2305-7068.2021.04.008.

Liu JT, Lou KX, Gao ZJ, Wang YB, Li Q, Tan MH. 2024. Comprehending hydrochemical fingerprint, spatial patterns, and driving forces of

groundwater in a topical coastal plain of Northern China based on hydrochemical and isotopic evaluations. Journal of Cleaner Production, 461, 142640. doi: 10.1016/j.jclepro.2024.142640.

Liu RN, Xie XJ, Hou QX, Han DY, Song JM, Huang GX. 2024. Spatial distribution, sources, and human health risk assessment of elevated nitrate levels in groundwater of an agriculture-dominant coastal area in Hainan Island, China. Journal of Hydrology, 634, 131088. doi: 10.1016/j.jhydrol.2024.131088.

Liu Y, Jiao JJ, Liang WZ, Kuang XX. 2017. Hydrogeochemical characteristics in coastal groundwater mixing zone. Applied Geochemistry, 85, 49–60. doi: 10.1016/j.apgeochem.2017.09.002.

Liu Y, Xue Q, Chang CW, Wang R, Liu ZY, He L. 2022. Recent progress regarding electrochemical sensors for the detection of typical pollutants in water environments. Analytical Sciences, 38(1), 55–70. doi: 10.2116/analsci.21SAR12.

Lu YX, Zhang JM. 2010. Quanzhou: Red, yellow and blue division of groundwater resources and dynamic management measures. China Water Resources, 17, 36–38 (in Chinese with English abstract). doi: 10.3969/j.issn.1000-1123.2010.17.017.

Luijendijk E, Gleeson T, Moosdorf N. 2020. Fresh groundwater discharge insignificant for the world's oceans but important for coastal ecosystems. Nature Communications, 11(1), 1260. doi: 10.1038/s41467-020-15064-8.

Luo MH, Zhang Y, Xiao K, Wang XJ, Zhang XL, Li G, Li HL. 2023. Effect of submarine groundwater discharge on nutrient distribution and eutrophication in Liaodong Bay, China. Water Research, 247, 120732. doi: 10.1016/j.watres.2023.120732.

Marandi A, Shand P. 2018. Groundwater chemistry and the Gibbs Diagram. Applied Geochemistry, 97, 209–212. doi: 10.1016/j.apgeochem.2018.07.009.

Matiatos I, Wassenaar LI, Monteiro LR, Venkiteswaran JJ, Gooddy DC, Boeckx P, Sacchi E, Yue FJ, Michalski G, Alonso-Hernández C, Biasi C, Bouchaou L, Edirisinghe NV, Fadhullah W, Fianko JR, García-Moya A, Kazakis N, Li SL, Luu MTN, Priyadarshanee S, Re V, Rivera DS, Romanelli A, Sanyal P, Tamooh F, Trinh DA, Walters W, Welti N. 2021. Global patterns of nitrate isotope composition in rivers and adjacent aquifers reveal reactive nitrogen cascading. Communications Earth and Environment, 2, 52. doi: 10.1038/s43247-021-00121-x.

Morici S, Gagliano Candela E, Favara R, La Pica L, Scaletta C, Pecoraino G. 2023. Hydrogeochemical characterization of the alluvial aquifer of Catania Plain, Sicily (South Italy). Environmental Earth Sciences, 82(6), 144. doi: 10.1007/s12665-023-10816-3.

Moussaoui I, Rosa E, Cloutier V, Neculita CM, Dassi L. 2023. Chemical and isotopic evaluation of groundwater salinization processes in the Djebeniana coastal aquifer, Tunisia. Applied Geochemistry, 149, 105555. doi: 10.1016/j.apgeochem.2022.105555.

Peng C, Gan MF, Che JL, Zhang Y, Shi P. 2024. Study on the influence of water exchange in river hyporheic zone on nitrogen migration and transformation process. Acta Ecologica Sinica, 44(23), 10794–10806 (in Chinese with English abstract). doi: 10.20103/j.stxb.20240202029.

Reyment RA, Davis JC. 1988. Statistics and data analysis in geology. Biometrics, 44(3), 918. doi: 10.2307/2531613.

Richardson CM, Davis KL, Ruiz-González C, Guimond JA, Michael HA, Paldor A, Moosdorf N, Paytan A. 2024. The impacts of climate change on coastal groundwater. Nature Reviews Earth & Environment, 5(2), 100–119. doi: 10.1038/s43017-023-00500-2.

Rodell M, Famiglietti JS, Wiese DN, Reager JT, Beaudoing HK, Landerer FW, Lo MH. 2018. Emerging trends in global freshwater availability. Nature, 557(7707), 651–659. doi: 10.1038/s41586-018-0123-1.

Rogers KM, van der Raaij R, Phillips A, Stewart M. 2023. A national isotope survey to define the sources of nitrate contamination in New Zealand freshwaters. Journal of Hydrology, 617, 129131. doi: 10.1016/j.jhydrol.2023.129131.

Santoni S, Huneau F, Garel E, Celle-Jeanton H. 2018. Multiple recharge processes to heterogeneous Mediterranean coastal aquifers and implications on recharge rates evolution in time. Journal of Hydrology, 559, 669–683. doi: 10.1016/j.jhydrol.2018.02.068.

Schroeter SA, Orme AM, Lehmann K, Lehmann R, Chaudhari NM, Küsel K, Wang H, Hildebrandt A, Totsche KU, Trumbore S, Gleixner G. 2025. Hydroclimatic extremes threaten groundwater quality and stability. Nature Communications, 16(1), 720. doi: 10.1038/s41467-025-55890-2.

Su C, Zhang FE, Cui XS, Cheng ZS, Zheng ZX. 2020. Source characterization of nitrate in groundwater using hydrogeochemical and multivariate statistical analysis in the Muling-Xingkai Plain, Northeast China. Environmental Monitoring and Assessment, 192(7), 456. doi: 10.1007/s10661-020-08347-6.

Su H, Li H, Chen H, Li Z, Zhang SH. 2023. Source identification and potential health risks of fluoride and nitrate in groundwater of a typical alluvial plain. Science of the Total Environment, 904, 166920. doi: 10.1016/j.scitotenv.2023.166920.

UNESCO. 2022. Groundwater: Making the invisible visible. United Nations. In: The United Nations World Water Development Report 2022: Paris, UNESCO, 34–35.

Wang D, Wu JH, Li PY, Li LX, Yang JY, Zhang PB, He S, Kou XM, Wang Y. 2024. Seasonal nitrate variations, risks, and sources in groundwater under different land use types in a thousand-year-cultivated region, northwestern China. Environmental Research, 251, 118699. doi: 10.1016/j.envres.2024.118699.

Wang H, Ni J, Song QC, Li C, Wang FG, Cao YQ. 2021. Analysis of coastal groundwater hydrochemistry evolution based on groundwater flow system division. Journal of Hydrology, 601, 126631. doi: 10.1016/j.jhydrol.2021.126631.

Wang SQ, Zhang ZX, Sprenger M, Wei SC, Zheng WB, Liu BB, Shen YJ, Zhang YZ. 2024. Seasonal recharge mechanism of the upper shallow groundwater in a long-term wastewater leakage and irrigation region of an alluvial aquifer. Journal of Hydrology, 629, 130424. doi: 10.1016/j.jhydrol.2023.130424.

Wang ZY, Li YL, Pan JB, Xu MY, Xu JJ, Hua DB. 2023. Array electrochemiluminescence device with ultra-high sensitivity and selectivity for rapid visualized monitoring of trace radon in environment. Journal of Hazardous Materials, 453, 131449. doi: 10.1016/j.jhazmat.2023.131449.

Wisitthammasri W, Chotpantarat S, Thitimakorn T. 2020. Multivariate statistical analysis of the hydrochemical characteristics of a volcano sedimentary aquifer in Saraburi Province, Thailand. Journal of Hydrology: Regional Studies, 32, 100745. doi: 10.1016/j.ejrh.2020.100745.

Wu CC, Cai F, Wu JZ, Zhao GG. 2011. Topographic and morphologic features in the coastal zone of Quanzhou Bay and their controlling factors. Marine Geology and Quaternary Geology, 31(4), 75–81. doi: 10.3724/SP.J.1140.2011.04075.

Yang Y, Yuan YL, Xiong GY, Yin ZY, Guo Y, Song J, Zhu XB, Wu JF, Wang JG, Wu JC. 2024. Patterns of nitrate load variability under surface water-groundwater interactions in agriculturally intensive valley watersheds. Water Research, 267, 122474. doi: 10.1016/j.watres.2024.122474.

Zamrsky D, Oude Essink GHP, Bierkens MFP. 2024. Global impact of sea level rise on coastal fresh groundwater resources. Earth's Future, 12(1), e2023EF003581. doi: 10.1029/2023EF003581.

Zhang AG, Liang Y, Ma R, 2024. Adsorption/desorption behavior of nh4-n under surface water-groundwater interaction and its impact on n migration and transformation. Earth Science, 49(10), 3761–3772 (in Chinese with English abstract). doi: 10.3799/dqkx.2023.188.

Zhang B, Song XF, Han DM, Guo ZR, Xiao GQ, Yang JL. 2013. Seawater intrusion degree evaluation based on mathematical

statistics and fuzzy mathematics in Qinhuangdao Yangdai River Plain. Scientia Geographica Sinica, 33(3), 342–348 (in Chinese with English abstract). doi: 10.13249/j.cnki.sgs.2013.03.342.

Zhang F, Wang JL, Huang DK, Zhong QQ, Yu T, Du JZ. 2023. Fresh groundwater discharge as a major source of ^{90}Sr into the coastal ocean. Environmental Science and Technology, 57(32), 12033–12041. doi: 10.1021/acs.est.3c03597.

Zhang HY, Han X, Wang GC, Mao HR, Chen XL, Zhou L, Huang DD, Zhang F, Yan X. 2023. Spatial distribution and driving factors of groundwater chemistry and pollution in an oil production region in the Northwest China. Science of The Total Environment, 875, 162635. doi: 10.1016/j.scitotenv.2023.162635.

Zhang M, Huang GX, Liu CY, Zhang Y, Chen ZY, Wang JC. 2020. Distributions and origins of nitrate, nitrite, and ammonium in various aquifers in an urbanized coastal area, south China. Journal of Hydrology, 582, 124528. doi: 10.1016/j.jhydrol.2019.124528.

Zhang Y, Chen ZY, Huang GX, Yang MN. 2023. Origins of groundwater nitrate in a typical alluvial-pluvial plain of North China plain: New insights from groundwater age-dating and isotopic fingerprinting. Environmental Pollution, 316, 120592. doi: 10.1016/j.envpol.2022.120592.

Zhao HM, Mao X, Liu CL, Li YS, Liu LJ. 2023. Transgression-regression processes since the MIS 3 in the coastal zone of Quanzhou Bay, Fujian. Journal of Geomechanics, 29(4), 569–583 (in Chinese with English abstract). doi: 10.12090/j.issn.1006-6616.2023046

Zheng R, Sun ZL, Jiao JG, Ma QQ, Zhao LQ. 2024. Salinity prediction based on improved LSTM model in the Qiantang Estuary, China. Journal of Marine Science and Engineering, 12(8), 1339. doi: 10.3390/jmse12081339.

Zhou J, Du Y, Deng YM, Tao YQ, Leng ZC, Ma T, Wang YX. 2022. Source identification of groundwater phosphorus under different geological settings in the central Yangtze River basin. Journal of Hydrology, 612, 128169. doi: 10.1016/j.jhydrol.2022.128169.

Zhu JC, Wang SB, Zheng ZQ. 2018. The Geological Survey Report of Quanzhou City. Southeast Fujian Geological Brigade, 96–106 (in Chinese).

Zhu YC, Yang HJ, Xiao Y, Hao QC, Li YS, Liu JH, Wang LW, Zhang YQ, Hu WX, Wang J. 2024. Identification of hydrochemical characteristics, spatial evolution, and driving forces of river water in Jinjiang Watershed, China. Water, 16(1), 45. doi: 10.3390/w16010045.